Analyst

PAPER

Cite this: *Analyst*, 2023, **148**, 3330

Effects of olanzapine and lithium carbonate antipsychotic agents on dopamine oxidation

Kaikai Han,[a] Jingjie Cui, *[a] Shaowei Chen [b] and Tao Yu[a]

Received 18th February 2023,
Accepted 18th May 2023

DOI: 10.1039/d3an00270e

rsc.li/analyst

Olanzapine (OLZ) and lithium carbonate (Li_2CO_3) are the main drugs for treating mental disorders related to dopamine (DA). A highly conductive carbon paper sensing electrode is used to investigate the effects of OLZ and Li_2CO_3 on DA oxidation due to its amplification of oxidation peak currents. Different chemical properties of drugs have different effects on DA oxidation. The presence of OLZ fouling on the electrode surface due to the irreversible adsorption weakens the sensing activity and thus reduces the DA oxidation peak current. However, the fixed DA oxidation peak potential at 0.22 V indicates no interaction between them. The hydrolysis effect of Li_2CO_3 increases the solution pH from 7.47 to 9.73, which promotes the deprotonation of DA, leading to a 156 mV negative shift of the DA oxidation peak potential. Additionally, a 94% decrease of the DA peak current may be related to the generation of polydopamine in alkaline media.

1. Introduction

Dopamine is a catecholamine[1,2] neurotransmitter in the central nervous system.[3,4] Abnormal release of dopamine can impact emotional stability[5] and lead to mental illnesses, such as schizophrenia[6] and bipolar disorder.[7] Olanzapine is considered one of the most effective drugs for sluggishly progressing schizophrenia,[8,9] which is an antagonist with a high affinity for dopamine receptors.[10,11] Meanwhile, lithium carbonate has been the first choice to stabilise the mood of patients suffering from bipolar disorder and prevent self-harm by significantly improving depression and anxiety.[12–14]

However, dopamine is readily oxidized when released from vesicles into the cytosol, and some oxidation products, such as semiquinone radicals, have been proposed to be highly toxic,[15] with adverse effects on the nervous system.[16,17] Hence, whether olanzapine and lithium carbonate have effects on the dopamine oxidation process has become an important issue. Although it is difficult to detect the oxidation of dopamine directly *in vivo*, the reaction is essentially a bioelectrochemical reaction. Electrochemical technology has the advantage of analyzing the redox properties of substances and can serve as a viable option for studying the effects of drugs on biomolecules *in vitro*. Ramadurai *et al.*[18] studied the interaction of the lipid membrane with ibuprofen and diclofenac drugs by electrochemical impedance tests (EIS). Ipte *et al.*[19] studied the interaction of ciprofloxacin and bovine serum albumin by differential pulse voltammetry (DPV). As the concentration of albumin increases, the oxidation peak current of the mixed solution decreases and the peak potential shifts forward, indicating an interaction between the drug and albumin. These achievements provide references for conducting electrochemical research about the effects of OLZ and Li_2CO_3 on DA oxidation.

The low oxidation peak current and adsorption contamination of drug molecules are the main challenges in electrochemical detection. Developing a sensing electrode that can amplify current signals and be easily updated is particularly important. Carbon paper is a disposable sensing material based on carbon fibers, where a high carbon content of over 90% enhances material conductivity[20] and cross-linked carbon fibers increase the specific surface area,[21,22] and these unique characteristics are beneficial for amplifying the current signals. In addition, unlike conventional materials that need a complex pre-treatment process, carbon paper only requires simple cleaning[23] to remove surface impurities prior to use. It is a renewable disposable sensing material with high availability in the electrochemical field.[24–26] And to our knowledge, so far, carbon paper has not been reported as a sensing electrode for studying the effect of antipsychotic drugs on DA oxidation.

In this work, a simple and efficient electrochemical sensor based on carbon paper was used to examine the effects of OLZ and Li_2CO_3 on DA oxidation. The organic functional groups of the carbon paper were analyzed by Fourier transform infrared spectroscopy (FT-IR), and the morphology of carbon paper was characterized by field emission scanning electron microscopy (FE-SEM). The electrochemical behaviors of dopamine[27,28] and

[a]*School of Automation, Hangzhou Dianzi University, Hangzhou, 310018, China*
[b]*Department of Chemistry and Biochemistry, University of California, 1156 High Street, Santa Cruz, California, 95064, USA. E-mail: cuijingjie@hdu.edu.cn*

drugs were studied by cyclic voltammetry (CV), and the electrochemical oxidation mechanism was briefly analyzed. Then, the effect of OLZ and Li_2CO_3 on DA oxidation was emphatically evaluated by square wave voltammetry (SWV).

2. Experimental

2.1. Materials

Dopamine (Macklin, Shanghai, China) and lithium carbonate (Aladdin, Shanghai, China) were dissolved in ultra-pure water. Olanzapine (Aladdin, Shanghai, China) was dissolved in anhydrous ethanol. 0.01 M phosphate buffered saline (PBS, pH 7.4; Macklin, Shanghai, China) was used as the supporting electrolyte. 0.1 M HNO_3 and 0.2 M NaOH are used to regulate the pH of PBS. All reagents were of analytical grade. Carbon paper was purchased from Toray (TGP-H-060, Toray, Japan). A 3 mm diameter glassy carbon electrode (GCE) was purchased from Ida (Tianjin, China).

2.2. Structural characterization of carbon paper

The infrared characterization of carbon paper was conducted using a Fourier transform infrared spectrometer (Prestise-21, China). The morphology of the carbon paper was examined by field emission scanning electron microscopy (Apreo S HiVac, China).

2.3. Preparation of the sensing electrode

The carbon paper was cleaned by ultrasonication in acetone, absolute ethanol and ultrapure water for 5 min successively to remove surface impurities, before being dried and cut into small pieces of 0.3 cm × 0.4 cm for later use. A GCE was polished with 0.5 μm alumina suspension until a mirror surface was obtained, and the carbon paper was fixed onto the GCE surface with 5 μL of Nafion solution (0.02% wt) and used after drying in the ambient environment for 6 h.

All electrochemical experiments were conducted on a CHI660C electrochemical workstation (CH Instruments, Shanghai, China) with carbon paper as the working electrode, an Ag/AgCl/KCl saturated reference electrode, and a platinum wire counter electrode. The parameters for SWV are as follows: initial potential *E*: 0.0 V; final potential *E*: 0.5/0.6 V; increasing potential: 0.004 V; amplitude: 0.025 V; frequency: 4 Hz.

3. Results and discussion

3.1. Structure characterization of carbon paper

The FT-IR spectrum of the carbon paper is shown in Fig. 1. The band at 3561 cm^{-1} was due to OH stretching,[29] likely arising from absorbed water on the sample. The broad peak at 2479 cm^{-1} can be ascribed to the stretching vibration of sulfhydryl (–SH) groups,[30] likely from the sulfur-containing materials used in the production of carbon paper. The peaks at 2185 cm^{-1} and 1996 cm^{-1} were ascribed to the stretching vibrations of nitrile[31] (C≡N) and carbonyl[32] (C═O), respectively. The weak peak at 1103 cm^{-1} may be due to the C–C skeleton vibration.[33] The peaks at 875 cm^{-1} and 536 cm^{-1} were ascribed to the bending vibrations of the C–H and C–C bonds of the benzene rings.[33] The active groups[34] such as sulfur and carbonyl groups help to increase the number of electrochemical active sites of carbon paper and improve the electrochemical sensing performance.

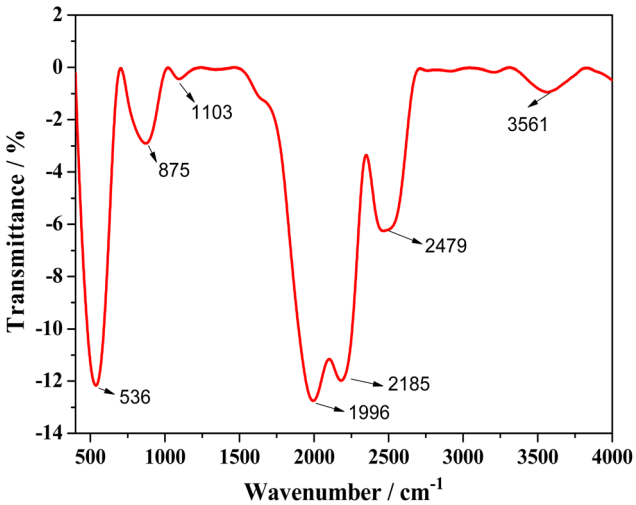

Fig. 1 FT-IR spectrum of carbon paper.

The surface morphology of the carbon paper was examined by FE-SEM. As shown in Fig. 2A, carbon fibers are randomly cross-distributed, forming a distinct stacked structure, and the long and straight fibers ensure the stability of the material. Further analysis of the microstructure indicates that carbon fibers possess a high carbon content and are in close contact with each other (Fig. 2B), which is conducive to electron transfer. The abundant interlayer voids increase the specific surface area of the material, which is conducive to the mass transfer process of the reactants (Fig. 2C). In addition, the edge sites formed by short and broken fibers can enhance the electrocatalytic activity (Fig. 2D), thereby accelerating the redox rate of biomolecules.[35–37]

3.2. Electrochemical behavior of DA

Cyclic voltammetry is a classical method to study the electroredox behavior of DA. Fig. 3A shows the CVs of 20 μM DA on carbon paper and a GCE, respectively, at a scan rate of 100 mV s^{-1}. DA exhibits one oxidation peak (0.205 V) and one reduction peak (0.154 V) on carbon paper, whereas on the GCE, the oxidation peak potential shifted slightly to 0.217 V. In fact, the DA oxidation peak current (3.22 μA) is higher on the carbon paper than that (0.62 μA) on the GCE, which indicates significant amplification of the DA oxidation peak current on the carbon paper due to the high conductivity. Additionally, carbon paper also exhibits a high background current due to its large capacitance properties.

Fig. 3B depicts the voltammograms of 20 μM DA on the carbon paper at different scanning rates. As the scan rate

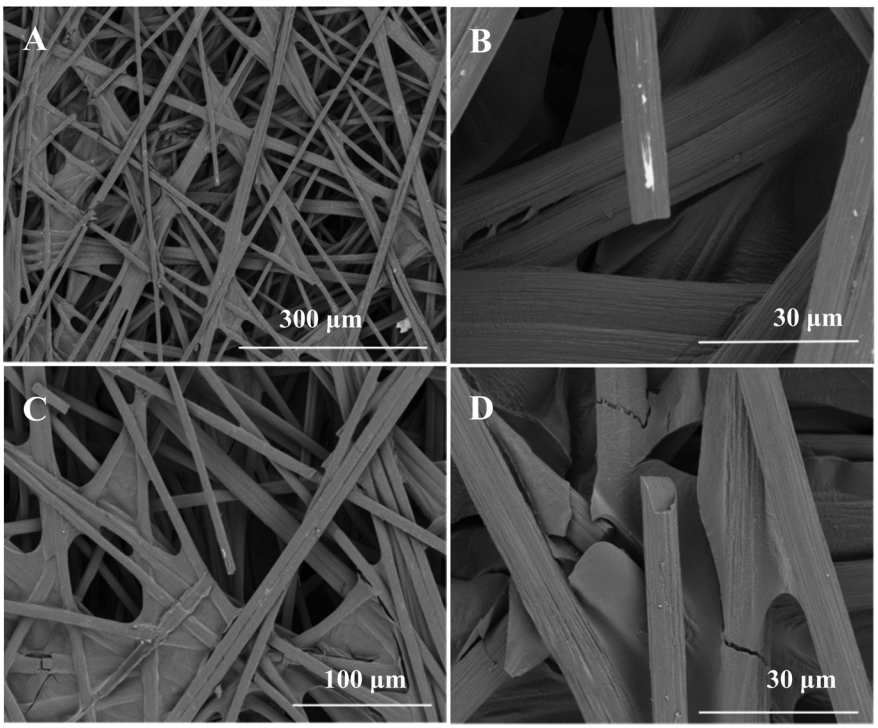

Fig. 2 FE-SEM images of carbon paper at different magnifications. Scale bars are (A) 300 μm, (C) 100 μm, and (B, D) 30 μm.

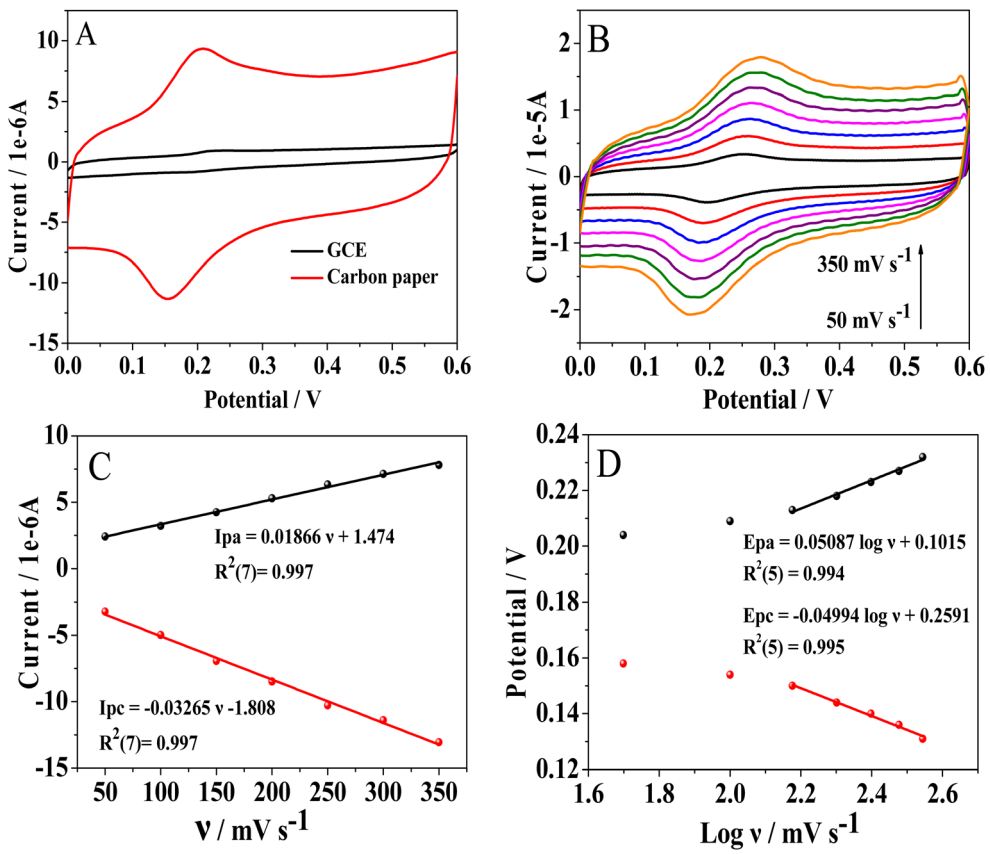

Fig. 3 (A) CVs of 20 μM DA on carbon paper and a GCE, respectively, in 0.01 M PBS at a scan rate of 100 mV s^{-1}. (B) CVs of 20 μM DA on carbon paper in the scan rate range of 50–350 mV s^{-1}. (C) Variation of the redox peak current *versus* the scan rate. (D) Variation of the redox peak potential *versus* the logarithm of scan rate.

increases, the peak splitting (ΔE_p) increases from 43 mV at 50 mV s^{-1} to 96 mV at 350 mV s^{-1}, compared to the theoretical value of 29.5 mV for a 2-electron process, suggesting a quasi-reversible reaction on the surface of the carbon paper. Moreover, as can be observed in Fig. 3C, the anodic and cathodic peak currents evolve linearly with the scan rate, which indicates that the electrochemical kinetics of DA on the carbon paper surface is adsorption controlled. The kinetic parameters could be evaluated based on Laviron's equations:[38,39]

$$E_{pc} = -\frac{2.3RT}{\alpha nF}\log \nu + \text{constant} \quad (1)$$

$$E_{pa} = \frac{2.3RT}{(1-\alpha)nF}\log \nu + \text{constant} \quad (2)$$

where R is the gas constant (8.314 J mol^{-1} K^{-1}), T is the temperature (291 K), the Faraday constant F is 96 485 C mol^{-1}, α is the electron-transfer coefficient, and n is the number of electron transfer. The plots shown in Fig. 3D demonstrate linearity between the logarithm of scan rate ($\log \nu$) and oxidation ($E_{pa_{DA}}$) and reduction ($E_{pc_{DA}}$) peak potential of DA, with the corresponding equations of $E_{pa_{DA}} = 0.05087 \log \nu + 0.1015$ ($R^2 = 0.994$, $N = 5$) and $E_{pc_{DA}} = -0.04994 \log \nu + 0.2591$ ($R^2 = 0.995$, $N = 5$), from which the values of α and n were determined to be 0.504 and 2.29, respectively, meaning that the electrooxidation process of DA involves 2-electron transfer.

Considering the pH influence on the electrooxidation process of DA, the change in the DA oxidation peak potential was studied in the pH range from 5.5 to 9.5. Fig. 4A shows that as the pH increases, the DA oxidation peak potential shifts from 324 mV to 76 mV, and Fig. 4B shows further analysis of the linear relationship between the oxidation peak potential and pH, and a regression equation of $E_{pa_{DA}} = -0.0608$ pH + 0.656 ($R^2 = 0.998$, $N = 9$) was obtained, with a slope of 60.8 mV pH^{-1}, which is close to the Nernstian theoretical value of 59 mV pH^{-1}.[40,41] This indicates that the same numbers of electrons and protons are involved in the process of DA electrooxidation.

The electrooxidation mechanism of DA in neutral media proposed in the literature[42–44] is illustrated in Scheme 1, where

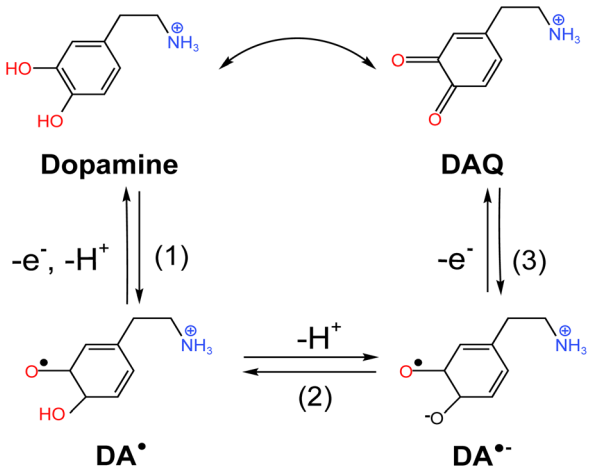

Scheme 1 Mechanism of DA electro-oxidation in 0.01 M PBS (pH 7.4).

DA first loses an electron and a hydrogen ion to form a neutral semiquinone radical (1), which will become an anionic radical with the loss of a second hydrogen ion (2), and after the loss of a second electron, the anionic radical is eventually oxidized to dopamine quinone (DAQ) (3). Many studies[45,46] have shown that the oxidation products of DA can bind to proteins such as α-synuclein, causing neurotoxicity or mitochondrial dysfunction, which is related to mental diseases.

3.3. Electrochemical behavior of OLZ

Voltammetric detection of 10 μM OLZ was performed in 0.01 M PBS within the potential window of 0 to 0.8 V at a scan rate of 100 mV s^{-1} on the carbon paper and GCE. The results are displayed in Fig. 5A. Compared with the weak electrochemical response on the GCE, OLZ displayed an obvious oxidation peak at 0.398 V and two reduction peaks at 0.150 V and 0.348 V on the carbon paper with a small peak splitting of only 50 mV. However, the broad oxidation peak suggests sluggish electron transfer kinetics.

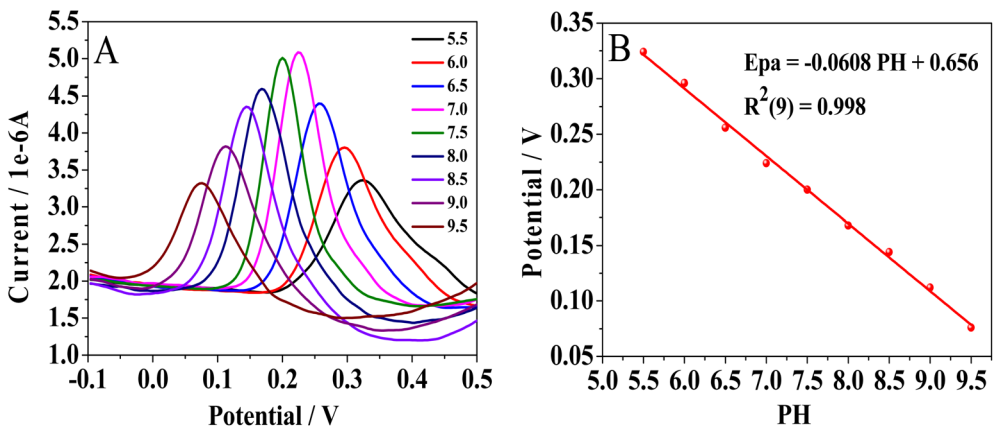

Fig. 4 (A) SWV curve of 20 μM DA in the pH range from 5.5 to 9.5 and (B) the linear relationship between pH and $E_{pa_{DA}}$.

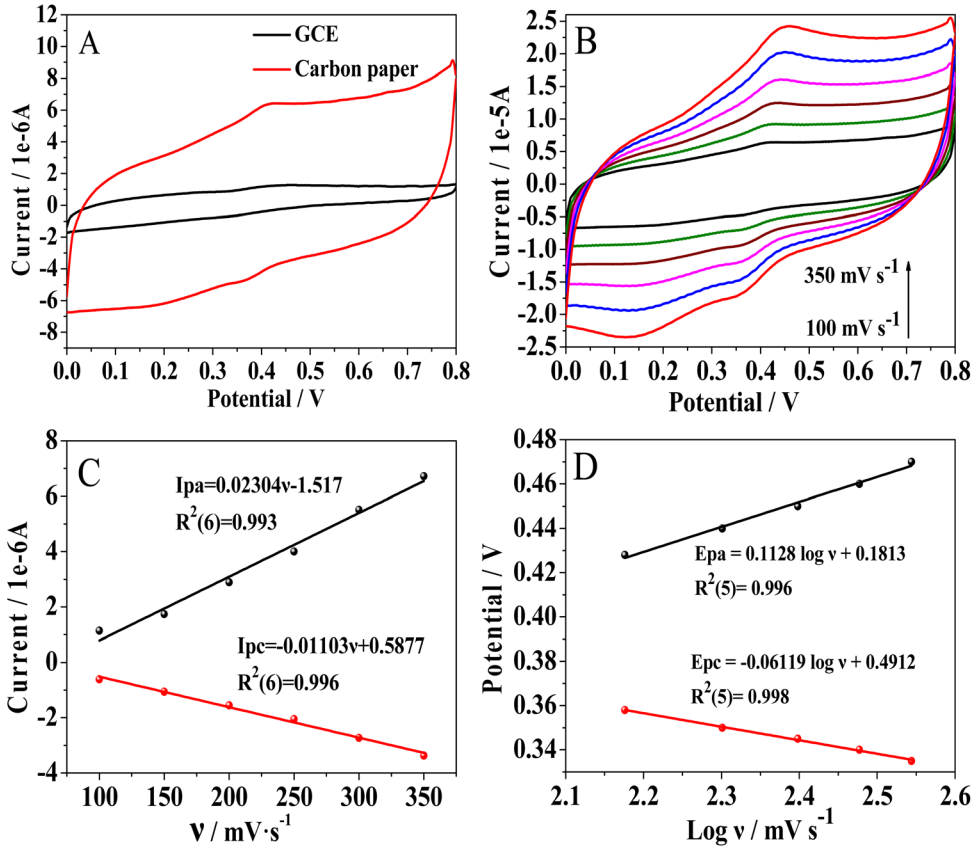

Fig. 5 (A) CVs of 10 μM OLZ on the carbon paper and GCE, in 0.01 M PBS at a scan rate of 100 mV s^{-1}. (B) CVs of 10 μM OLZ on the carbon paper at different scan rates of 100–350 mV s^{-1}. (C) Plot of redox peak current *versus* the scan rate (ν). (D) Plot of redox peak potential *versus* the log ν.

The influence of scan rates on the OLZ oxidation kinetics was then studied by CV. It can be observed from Fig. 5B that the OLZ oxidation peak potential (0.398 V) has shifted positively while the cathodic peak potential (0.348 V) has shifted negatively with the scan rate increasing from 100 to 350 mV s^{-1}. Meanwhile, ΔE_p is observed to increase from 70 mV to 135 mV, compared to the 59.2 mV for a 1-electron process, indicating a kinetically quasi-reversible reaction with increasing scan rates. This may be due to the irreversible adsorption of OLZ molecules onto the carbon paper electrode surface and sluggish electron transfer kinetics. As Fig. 5C reveals, the oxidation ($I_{pa_{OLZ}}$) and reduction ($I_{pc_{OLZ}}$) peak currents of OLZ increased gradually with increasing scan rates (ν), and the linear equations are $I_{pa_{OLZ}} = 0.02304\ \nu - 1.517$ ($R^2 = 0.993$, $N = 6$) and $I_{pc_{OLZ}} = -0.01103\ \nu + 0.5877$ ($R^2 = 0.996$, $N = 6$), suggesting that the electrochemical reaction of OLZ on the carbon paper is surface adsorption-controlled. In addition, linear relationships (Fig. 5D) were observed between the redox peak potentials ($E_{pa_{OLZ}}$ and $E_{pc_{OLZ}}$) and $\log \nu$, $E_{pa_{OLZ}} = 0.1128 \log \nu + 0.1813$ ($R^2 = 0.996$, $N = 5$) and $E_{pc_{OLZ}} = -0.06119 \log \nu + 0.4912$ ($R^2 = 0.998$, $N = 5$). The values of α and n based on eqn (1) and (2) were determined to be 0.64 and 1.3, demonstrating that the electro-oxidation process of OLZ involved one electron transfer, in good accordance with the results reported by Muthusankar *et al.*[47] and Merli *et al.*[48] Scheme 2 shows the mechanism of electrochemical oxidation

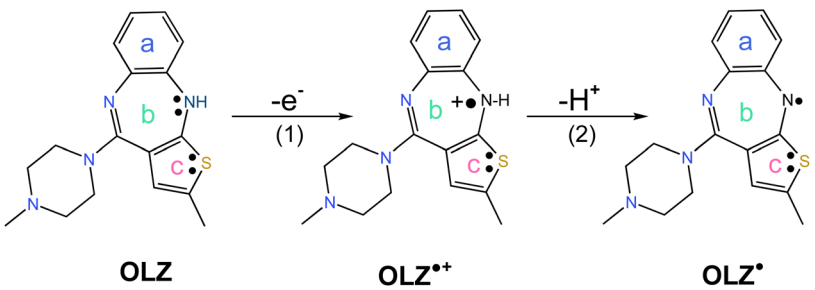

Scheme 2 Mechanism of OLZ electro-oxidation.

of OLZ.[47–49] An olanzapine molecule contains three unsaturated rings, with an aromatic benzene ring (a) and a thiophene ring (c). Such a stable structure makes the oxidation reaction difficult. The seven-membered nitrogen heterocycle (b) has no aromaticity, with weakened stability and acidity. Therefore, during the electro-oxidation process of OLZ, the –NH group on the nitrogen heterocycle first loses an electron (1), leading to OLZ oxidation into a free radical cation, increased molecular acidity,[50] dissociation of hydrogen ions (2), and ultimately conversion into a neutral free radical.

3.4. Simultaneous determination of DA and OLZ

The interaction between OLZ on DA was then studied by SWV in 0.01 M PBS solution. The concentration of DA was fixed at 20 μM, and then OLZ was added at increasing concentrations from 1 μM to 10 μM. Fig. 6A shows the changes of their electrochemical responses. From the perspective of peak current, as the concentration of OLZ increases, the oxidation peak current of DA continues to decrease, which indicates that the addition of OLZ weakens the electrochemical response of DA. Fig. 6C shows that the DA oxidation peak current decreases linearly with the increase of OLZ concentration (C_{OLZ}), with a regression equation of $I_{pa_{DA}} = -0.1796\ C_{OLZ} + 2.909$ ($R^2 = 0.998$, $N = 11$). However, the change of the oxidation peak current of OLZ is different from that of DA. The OLZ oxidation peak current increases from 41 nA to 153 nA within the concentration range of 1 to 6 μM. A further increase in the concentration (7–10 μM) leads to a decrease of the OLZ oxidation peak current from 153 nA to 105 nA. That is, DA and OLZ exhibit different current variations. As described above, the lack of aromaticity of the seven-member nitrogen heterocycle (Scheme 2) in OLZ makes it difficult to oxidize. Additionally, fouling occurred on the electrode surface due to the irreversible adsorption of OLZ molecules. These cause severe restrictions in the electrochemical reactions of DA and OLZ.

Fouling of electrodes has been observed with OLZ,[47–49] as manifested by the diminishment of the OLZ oxidation peak current under continuous cyclic voltammetry detection. Fig. 6B depicts 40 cycles of voltammetric scans of 20 μM OLZ, where one can see that the OLZ oxidation peak current decreased by 93%, from 1.45 μA (first cycle) to 0.1 μA (fortieth cycle), indicating that OLZ fouling indeed occurred on the surface of the carbon paper electrode, which is consistent with the literature.[49] Therefore, electrode pollution caused by OLZ is the reason for changes in the oxidation peak current of DA and OLZ. The increase in the concentration of OLZ deepens the degree of electrode pollution, prompting a continuous decrease of DA oxidation peak current. Meanwhile, the OLZ

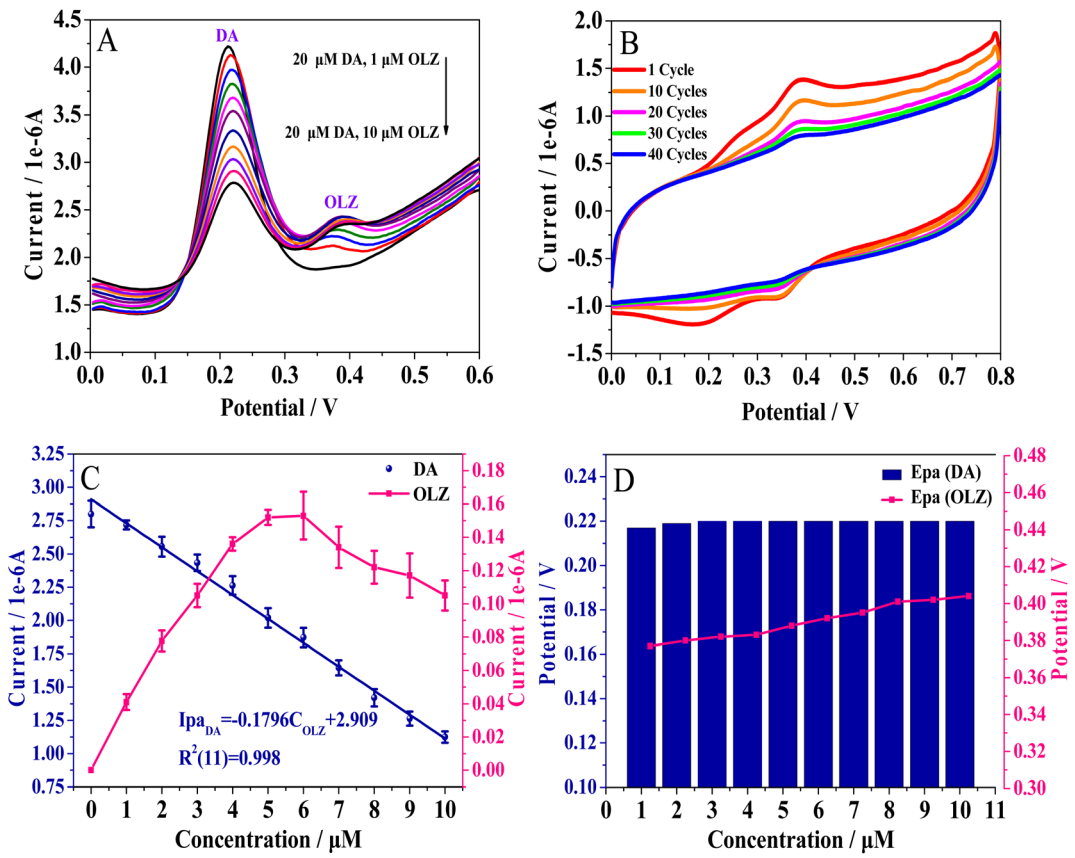

Fig. 6 (A) SWVs of 20 μM DA and 1–10 μM OLZ; (B) CVs of 20 μM OLZ in 1–40 cycles at a scan rate of 100 mV s^{-1}; (C) plots of the oxidation peak current of DA and OLZ as a function of OLZ concentration; and (D) plots of the oxidation peak potential of DA and OLZ as a function of OLZ concentration.

oxidation peak current also shows a trend of first increasing and then decreasing.

On the other hand, the peak potential also exhibits different changes (Fig. 6D). The oxidation peak potential of DA remained at 0.22 V and was not affected by OLZ, suggesting that the oxidation process of DA and OLZ is independent and there is no interaction between them. It is worth noting that the OLZ oxidation peak potential shifted from 0.377 V at 1 μM to 0.402 V at 10 μM, also due to OLZ contamination of the electrode that weakened the electro-oxidation ability to olanzapine.

3.5. Electrochemical behavior of lithium carbonate

The electrochemical behavior of lithium carbonate was studied by CV in the potential range from 0.8 to 1.8 V. From Fig. 7A it can be seen that Li_2CO_3 exhibits a high oxidation peak (1.5 V) on the carbon paper without a reduction peak, indicating that the electrooxidation of Li_2CO_3 is an irreversible reaction. The electrode kinetics of Li_2CO_3 were studied at different scan rates ranging from 50 to 300 mV s^{-1}, as shown in Fig. 7B. As the scan rate increases, the peak current of Li_2CO_3 oxidation increases from 0.19 mA to 0.32 mA, and the peak potential of oxidation increases from 1.49 V to 1.53 V. After linear fitting of the oxidation peak current ($I_{pa_{Li}}$) of Li_2CO_3 and the square root of the scan rate ($\nu^{1/2}$), the regression equation can be expressed as $I_{pa_{Li}} = 0.1295\ \nu^{1/2} + 0.9567$ ($R^2 = 0.996$, $N = 6$), demonstrating the diffusion nature of the electrochemical lithium carbonate reaction (Fig. 7C), and the corresponding diffusion coefficient can be obtained through the Randles–Sevcik irreversible system diffusion control equation:[51]

$$I_{pa} = 2.99 \times 10^5\ n\ [(1-\alpha)\ n]^{1/2} A\ C_0\ D_0^{1/2}\ \nu^{1/2} \quad (3)$$

where A is the effective surface area of the carbon paper, C_0 is the concentration of Li_2CO_3, D_0 is the diffusion coefficient, and ν is the scan rate. Fig. 7D shows a linear correlation between the logarithm of scan rate ($\log \nu$) and the oxidation peak potential ($E_{pa_{Li}}$) of Li_2CO_3 as $E_{pa_{Li}} = 0.0539 \log \nu + 1.386$ ($R^2 = 0.997$, $N = 6$), and in combination with eqn (2), the value of $(1-\alpha)\ n$ can be calculated to be 0.95. By substituting 0.95 and values of other parameters (A, C_0) in eqn (3), the diffusion coefficient D_0 of Li_2CO_3 can be calculated to be 8.593×10^{-9} $cm^2\ s^{-1}$.

Lithium carbonate is a strong base–weak acid salt, which is prone to hydrolysis in aqueous media. In the reaction mechanisms shown in Scheme 3, Li_2CO_3 is first ionized into the lithium ion and carbonate anion (1), then the carbonate anion

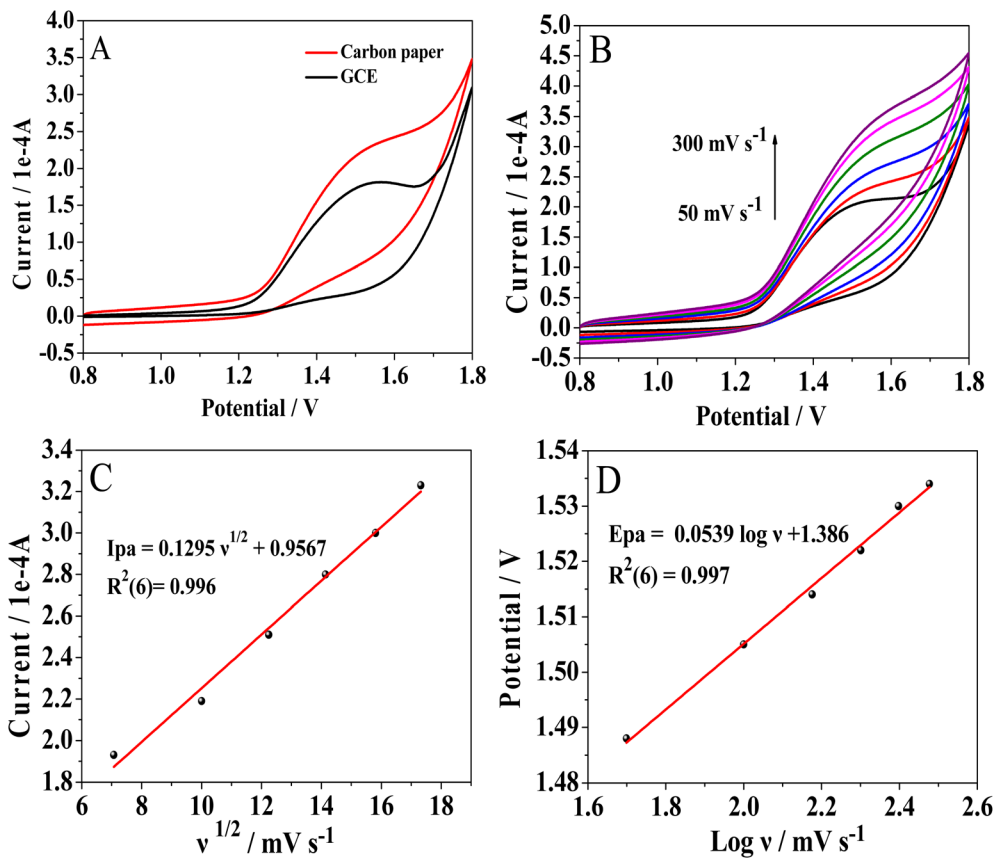

Fig. 7 (A) CVs of 20 mM Li_2CO_3 on carbon paper and GCE, in 0.01 M PBS at a scan rate of 100 mV s^{-1}. (B) CVs of 20 mM Li_2CO_3 on carbon paper at different scan rates of 50–300 mV s^{-1}. (C) Plot of the Li_2CO_3 oxidation peak current *versus* $\nu^{1/2}$. (D) Plot of Li_2CO_3 oxidation peak potential *versus* $\log \nu$.

$$Li_2CO_3 \longrightarrow 2Li^+ + CO_3^{2-} \quad (1)$$

$$CO_3^{2-} + H_2O \longrightarrow HCO_3^- + OH^- \quad (2)$$

$$HCO_3^- + H_2O \longrightarrow H_2CO_3 + OH^- \longrightarrow H_2O + CO_2 + OH^- \quad (3)$$

$$O_2 + e^- \longrightarrow O_2^{\bullet-} \quad (4)$$

$$2O_2^{\bullet-} + H_2O \longrightarrow HO_2^- + OH^- + O_2 \quad (5)$$

$$Li_2CO_3 + 2H_2O + O_2^{\bullet-} \longrightarrow 2Li^+ + 3OH^- + CO_2 + HO_2^- \quad (6)$$

$$2HO_2^- \longrightarrow 2OH^- + O_2 \quad (7)$$

Scheme 3 Mechanism of Li_2CO_3 hydrolysis and electro-oxidation.

is hydrolyzed into the hydroxide ion and bicarbonate anion (2), and the bicarbonate is further hydrolyzed to produce OH^- (3), which makes the solution alkaline and pH increases. In addition, in the presence of air, the aqueous solution undergoes an oxygen reduction reaction[52,53] under the action of an electric field to generate superoxide radicals (4). The superoxide radicals continue to react with water in an alkaline medium to generate the hydrogen peroxide anion (HO^{2-}), while oxygen is released (5). Therefore, the hydrolysis and electrooxidation mechanisms of lithium carbonate can be summarized as reactions in (6) and (7), and the hydrolysis of strong alkali weak acid salt lithium carbonate generates a large amount of OH^-, forming an alkaline environment.

3.6. Simultaneous determination of DA and Li_2CO_3

In order to study the effect of lithium carbonate on the electrochemical response of dopamine, SWV was used to simultaneously detect DA and Li_2CO_3 in 0.01 M PBS. In the experiment, the concentration of DA was kept constant at 20 μM, and 0.1–0.7 mM Li_2CO_3 was continuously increased to examine the changes of the electrochemical response. The results are shown in Fig. 8A, where the oxidation peak potential of DA shows a negative shift, while the DA oxidation peak current significantly decreases, with the increase of Li_2CO_3 concentration. Fig. 8C and D specifically show the analysis of the changes in the DA oxidation peak potential and oxidation peak current. Following the sequential increase of Li_2CO_3 (0.1–0.7 mM), the DA oxidation peak potential began to shift negatively from 0.216 V to 0.06 V, with a potential shift of 156 mV. At the same time, the DA oxidation peak current decreased by 94% (from 1.612 μA to 0.102 μA), indicating that the addition of Li_2CO_3 had a significant impact on DA oxidation.

The change of pH will easily affect the protonation of DA, causing the shift of the oxidation peak potential, which has

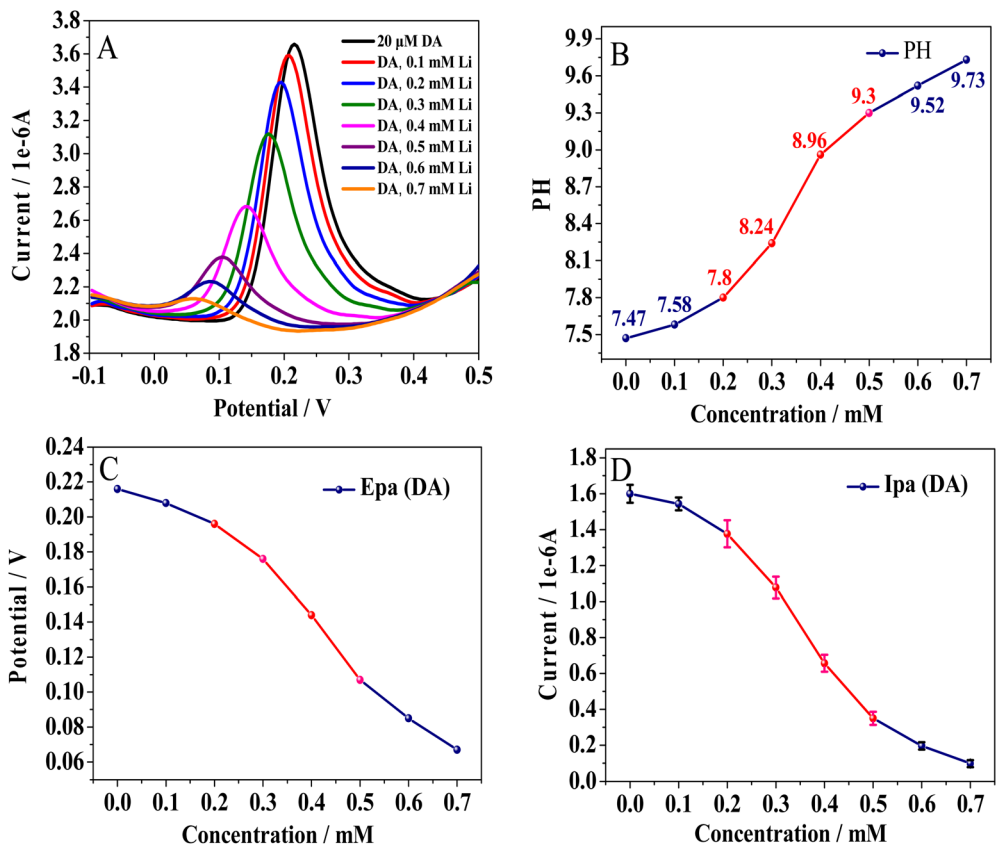

Fig. 8 (A) Square wave voltammograms of 20 μM DA, in the presence of 0.1–0.7 mM Li_2CO_3, at the carbon paper electrode in 0.01 M PBS. (B) Plot of solution pH and Li_2CO_3 concentration; (C) plot of the DA oxidation peak current and Li_2CO_3 concentration; and (D) plot of the DA oxidation peak potential and Li_2CO_3 concentration.

been proven previously in DA electrooxidation (Fig. 4). Considering that the hydrolysis of Li_2CO_3 to generate OH^- can easily increase the solution pH (Scheme 3), perhaps the change in DA electrooxidation behavior is related to this. For this purpose, we detected the pH value changes of the mixed solution, and the results are shown in Fig. 8B. As the concentration of Li_2CO_3 increases from 0.1 mM to 0.7 mM, the pH value gradually increases from 7.47 to 9.73. Furthermore, it can be found that the trend of changes in DA oxidation peak potential (Fig. 8C) and oxidation peak current (Fig. 8D) is very consistent with the change in pH (Fig. 8B). When the concentration of Li_2CO_3 increases from 0 to 0.2 mM, the increase of the pH value is only 0.33, the negative shift of the DA peak potential is only 20 mV, and the decrease in DA peak current is 0.2 μA. However, as the concentration of Li_2CO_3 increases from 0.2 mM to 0.5 mM, the solution pH rapidly increases from 7.8 to 9.3, and the DA oxidation peak potential and peak current also show the most significant negative shift (90 mV) and the maximum current decrease (1.06 μA). As the concentration of Li_2CO_3 continued to increase to 0.7 mM, the increase in solution pH tended to slow down, and correspondingly, the shift in DA oxidation peak potential (40 mV) and the decrease in peak current (0.27 μA) also began to decrease. These results all indicate that the increase in solution pH caused by the hydrolysis of Li_2CO_3 is the reason for the negative shift of the DA oxidation peak potential and the decrease in the oxidation peak current.

The shift of the DA oxidation peak potential is related to deprotonation, but the reason for the decrease in DA oxidation peak current is worth further exploration, which may be related to the generation of polydopamine in alkaline media. Dopamine contains one amino function that can be protonated and two phenolic groups that can dissociate, so the solution pH has a great influence on the oxidation of DA. At a low pH value, it is difficult to deprotonate the phenolic group while the amino group can be easily protonated.[54,55] However, as the solution pH increases, the deprotonation of the phenolic group becomes easier, while the protonation of the amino group becomes more difficult, resulting in two outcomes, as shown in Scheme 4.[56,57] One is that DA is more likely to be oxidized to dopamine quinone (DAQ) (1), leading to the increase of the DA oxidation peak current. The other is that the deprotonation of the amino group is conducive to intramolecular cyclization[58] of DAQ to produce leucodopaminechrome (LDAC) (2), which can generate polydopamine through the subsequent reaction (3). Polydopamine, as a strong adhesive substance,[59] will passivate the electrode,[60] resulting in a decrease of sensing performance, diminishing the DA oxidation peak current. Thus, the DA oxidation peak current will depend on the dual effects of deprotonation and passivation, which is demonstrated in Fig. 9A. In the pH range of 5.5–7.0, the DA oxidation peak current increases with the increase of pH, and the DA oxidation peak potential also moves negatively, which indicates that the increase of pH promotes the deprotonation of DA. However, when the solution pH exceeds 7.5, the DA oxi-

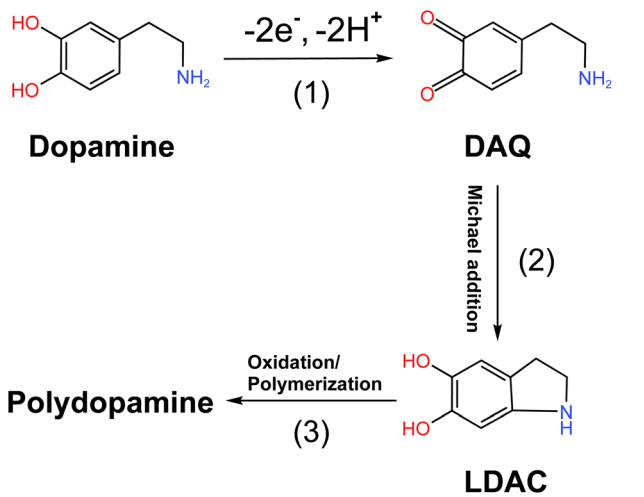

Scheme 4 A brief mechanism for the formation of polydopamine in alkaline media.

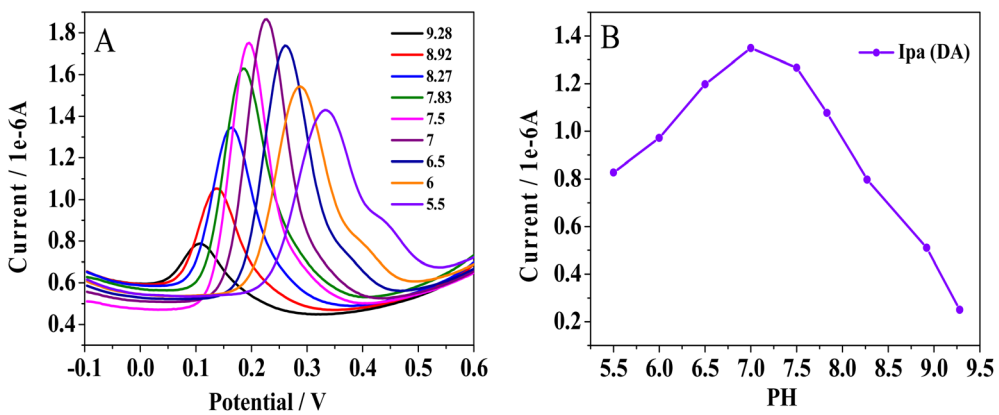

Fig. 9 (A) SWV diagram of 20 μM dopamine on the carbon paper electrode, the pH of the solution was adjusted by the addition of 0.1 M nitric acid and 0.1 mM Li_2CO_3, respectively and (B) plot of the DA oxidation peak current and pH.

dation peak current does not increase with the acceleration of deprotonation, but decreases (Fig. 9B). It is likely that the formation of polydopamine has a passivation effect on the electrode. The literature[55,61] has shown that when the pH value is greater than 7, dopamine can rely on the dissolved oxygen in the solution to generate polydopamine, which becomes easier under electrooxidation conditions.[62,63] Therefore, it can be inferred that the addition of Li_2CO_3 leads to the continuous increase of pH (from 7.47 to 9.73), which promotes the formation of polydopamine and leads to electrode passivation. This passivation effect exceeds the deprotonation effect, so that the dopamine oxidation peak current decreases in alkaline media. This will be further studied in the future.

4. Conclusions

In summary, the effects of OLZ and Li_2CO_3 on DA oxidation were studied using a high conductivity carbon paper electrode. The electrode fouling from OLZ and the hydrolysis effect of Li_2CO_3 have different effects on DA oxidation. The presence of OLZ results in significant fouling of the carbon paper, hindering the DA oxidation process. However, the unchanged DA oxidation peak potential (0.22 V) indicates that no interaction occurs between them. The hydrolysis of Li_2CO_3 increased the solution pH from 7.47 to 9.73, making the DA oxidation peak potential negatively shift from 0.216 V to 0.06 V. Additionally, the 94% decrease in the DA oxidation peak current may be related to the formation of polydopamine due to high pH. The passivation electrode of polydopamine causes a decrease in the peak current of DA.

Author contributions

Kaikai Han: Writing – original draft, investigation, data curation, visualization, and formal analysis. Jingjie Cui: Conceptualization, resources, data curation, software, formal analysis, supervision, methodology, writing – original draft, and project administration. Shaowei Chen: writing – review and editing. Tao Yu: writing – review and editing.

Conflicts of interest

There are no conflicts of interest to declare.

Acknowledgements

This work was supported by the Zhejiang Province Public Welfare Technology Application Research Project (LGF19E020002) and the National Natural Science Foundation of China (51102152).

References

1 F. Fornai and S. Puglisi-Allegra, *Neurosci. Biobehav. Rev.*, 2021, **123**, 238–256.
2 A. G. Golubev, *Ageing Res. Rev.*, 2022, **75**, 101570.
3 I. O. Blokhin, O. Khorkova, R. V. Saveanu and C. Wahlestedt, *Neurobiol. Dis.*, 2020, **146**, 105136.
4 C. Missale, S. R. Nash, S. W. Robinson, M. Jaber and M. G. Caron, *Physiol. Rev.*, 1998, **78**, 189–225.
5 K. P. Morie, M. J. Crowley, L. C. Mayes and M. N. Potenza, *J. Psychiatr. Res.*, 2022, **148**, 264–274.
6 R. A. McCutcheon, T. R. Marques and O. D. Howes, *JAMA Psychiatry*, 2020, **77**, 201–210.
7 B. J. Overs, R. K. Lenroot, G. Roberts, M. J. Green, C. Toma, D. Hadzi-Pavlovic, K. D. Pierce, P. R. Schofield, P. B. Mitchell and J. M. Fullerton, *Psychiatry Res., Neuroimaging*, 2021, **309**, 111258.
8 J. J. Ren and C. Zhang, *Asian J. Psychiatry*, 2021, **62**, 102741.
9 B. Birur, J. Thirthalli, N. Janakiramaiah, R. C. Shelton and B. N. Gangadhar, *Asian J. Psychiatry*, 2016, **24**, 17–22.
10 J. M. Lian, X. F. Huang, N. Pai and C. Deng, *Prog. Neuro-Psychopharmacol. Biol. Psychiatry*, 2013, **47**, 62–68.
11 A. Chen and H. Nasrallah, *Schizophr. Res.*, 2019, **208**, 1–7.
12 G. Jones, C. Rong, C. M. Vecera, C. I. Gurguis, R. Chudal, R. Khairova, E. Leung, A. C. Ruiz, L. Shahani, M. V. Zanetti, R. T. de Sousa, G. Busatto, J. Soares, W. F. Gattaz and R. Machado-Vieira, *J. Affective Disord.*, 2022, **308**, 71–75.
13 A. Khayachi, L. Schorova, M. Alda, G. A. Rouleau and A. J. Milnerwood, *Neurosci. Biobehav. Rev.*, 2021, **127**, 424–445.
14 Y. Uwai and T. Nabekura, *J. Psychiatr. Res.*, 2022, **153**, 99–103.
15 S. Latif, M. Jahangeer, D. M. Razia, M. Ashiq, A. Ghaffar, M. Akram, A. El Allam, A. Bouyahya, L. Garipova, M. Ali Shariati, M. Thiruvengadam and M. A. Ansari, *Clin. Chim. Acta*, 2021, **522**, 114–126.
16 R. M. Wise, A. Wagener, U. M. Fietzek, T. Klopstock, E. V. Mosharov, F. A. Zucca, D. Sulzer, L. Zecca and L. F. Burbulla, *Neurobiol. Dis.*, 2022, **175**, 105920.
17 O. Terland, B. Almås, T. Flatmark, K. K. Andersson and M. Sørlie, *Free Radical Biol. Med.*, 2006, **41**, 1266–1271.
18 S. Ramadurai, N. K. Sarangi, S. Maher, N. MacConnell, A. M. Bond, D. McD-aid, D. Flynn and T. E. Keyes, *Langmuir*, 2019, **35**, 8095–8109.
19 P. R. Ipte, S. Sahoo and A. K. Satpati, *Bioelectrochemistry*, 2019, **130**, 107330.
20 Á. Torrinha and S. Morais, *TrAC, Trends Anal. Chem.*, 2021, **142**, 116324.
21 H. Shi, G. Wen, Y. Nie, G. Zhang and H. Duan, *Nanoscale*, 2020, **12**, 5261–5285.
22 S. Ghosh and R. N. Basu, *Nanoscale*, 2018, **10**, 11241–11280.
23 H. S. Yang, J. Bao, Y. L. Qi, J. Y. Zhao, Y. Hu, W. X. Wu, X. C. Wu, D. D. Zhong, D. Q. Huo and C. J. Hou, *Anal. Chim. Acta*, 2020, **1135**, 12–19.
24 M. C. Radulescu, M. P. Bucur, B. Bucur and G. L. Radu, *Talanta*, 2019, **199**, 541–546.

25 L. Yan, P. C. Ma, Y. C. Liu, X. Y. Ma, F. Chen and M. Q. Li, *Microchem. J.*, 2020, **159**, 105347.
26 K. B. Akshaya, V. Anitha, M. Nidhin, Y. N. Sudhakar and G. Louis, *Talanta*, 2020, **217**, 121028.
27 S. Shahrokhian and S. Bozorgzadeh, *Electrochim. Acta*, 2006, **51**, 4271–4276.
28 S. Mikko, M. Lauri, K. Henri, O. Tuomo and L. Jukka, *J. Phys. Chem. B*, 2018, **122**, 6314–6327.
29 D. S. Yuan, X. R. Chen, Z. Y. Li, C. Fang, J. Ding, H. Wan and G. Guan, *Appl. Surf. Sci.*, 2021, **569**, 151089.
30 R. Raj, K. Dalei, J. Chakraborty and S. Das, *J. Colloid Interface Sci.*, 2016, **462**, 166–175.
31 T. T. B. Tran, E. J. Park, H. Kim, H. J. Jang and J. T. Son, *Mater. Chem. Phys.*, 2022, **290**, 126590.
32 C. A. Bode-Aluko, O. Pereao, H. H. Kyaw, L. Al-Naamani, C. A. Bode-Aluko, O. Pereao, H. H. Kyaw, L. Al-Naamani, M. Z. Al-Abri, M. T. Z. Myint, A. Rossouw, O. Fatoba, L. Petrik and S. Dobretsov, *J. Mater. Sci. Eng. B*, 2021, **264**, 114913.
33 L. M. Lepodise and R. Bosigo, *Spectrochim. Acta, Part A*, 2022, **267**, 120469.
34 S. Biswas, P. Roy, S. Jana and T. K. Mondal, *J. Organomet. Chem.*, 2017, **846**, 201–207.
35 P. P. Wei, J. Shen, K. B. Wu and N. J. Yang, *Carbon*, 2019, **154**, 125–131.
36 C. X. Xu, Z. Li, L. Y. Yang, L. Y. Hu, W. Wang, J. L. Huang, H. H. Zhou, L. Chen and Z. H. Hou, *J. Electroanal. Chem.*, 2022, **923**, 116826.
37 L. Wang and M. Pumera, *Appl. Mater. Today*, 2016, **5**, 134–141.
38 E. Laviron, *J. Electroanal. Chem. Interfacial Electrochem.*, 1979, **101**, 19–28.
39 X. J. Zhang and J. B. Zheng, *Sens. Actuators, B*, 2019, **290**, 648–655.
40 F. Nosratzehi, H. Halakoei, M. Rostami, A. Sorouri, K. Adib, M. R. Nasrabadi and H. Ehrlich, *Diamond Relat. Mater.*, 2022, **127**, 109120.
41 A. H. Mehrjardi, M. A. Karimi, M. Soleymanzadeh and A. Barani, *Measurement*, 2020, **163**, 107893.
42 J. Jiang, Y. C. Cao, J. L. Liu, H. Zhang, G. F. Kan and K. Yu, *Anal. Chim. Acta*, 2022, **1193**, 339403.
43 M. Salomaki, L. Marttila, H. Kivela, T. Ouvinen and J. Lukkari, *J. Phys. Chem. B*, 2018, **122**, 6314–6327.
44 I. Iftikhar, K. M. Abou El-Nour and A. Brajter-Toth, *Electrochim. Acta*, 2017, **249**, 145–154.
45 A. Biosa, I. Arduini, M. E. Soriano, V. Giorgio, P. Bernardi, M. Bisaglia and L. Bubacco, *ACS Chem. Neurosci.*, 2018, **9**, 2849–2858.
46 E. Monzani, S. Nicolis, S. Dell'Acqua, A. Capucciati, C. Bacchella, E. Monzani, S. Nicolis, S. Dell'Acqua, A. Capucciati, C. Bacchella, F. A. Zucca, E. V. Mosharov, D. Sulzer, L. Zecca and L. Casella, *Angew. Chem., Int. Ed.*, 2019, **58**, 6512–6527.
47 G. Muthusankar, A. Sangili, S. M. Chen, R. Karkuzhali, M. Sethupathi, G. Gopu, S. Karthick, R. K. Devi and N. Sengottuvelan, *J. Mol. Liq.*, 2018, **268**, 471–480.
48 D. Merli, D. Dondi, M. Pesavento and A. Profumo, *J. Electroanal. Chem.*, 2012, **683**, 103–111.
49 J. I. Gowda, R. M. Hanabaratti, P. D. Pol, R. C. Sheth, P. P. Joshi and S. T. Nandibewoor, *Chem. Data Collect.*, 2022, **38**, 100824.
50 S. Shahrokhian, M. Azimzadeh and P. Hosseini, *RSC Adv.*, 2014, **4**, 40553–40560.
51 A. J. Bard, L. R. Faulkner, A. Bard and L. Faulkner, *Electrochemical Methods: Fundamentals and Applications*, Wiley, New York, 2nd edn, 2001.
52 X. W. Chi, Y. G. Tang and X. Q. Zeng, *Eletrochim. Acta*, 2016, **216**, 171–180.
53 A. S. Workman, *Comput. Theor. Chem.*, 2017, **1117**, 207–214.
54 A. E. Sánchez-Rivera, S. Corona-Avendaño, G. Alarcón-Angeles, A. Rojas-Hernández and M. T. Ramírez-Silva, *Spectrochim. Acta, Part A*, 2003, **59**, 3193–3203.
55 S. Schindler and T. Bechtold, *J. Electroanal. Chem.*, 2019, **836**, 94–101.
56 Y. L. Li, M. L. Liu, C. H. Xiang, Q. J. Xie and S. Z. Yao, *Thin Solid Films*, 2006, **497**, 270–278.
57 L. C. Almeida, R. D. Correia, A. Marta, G. Squillaci, A. Morana, F. La Cara, J. P. Correia and A. S. Viana, *Appl. Surf. Sci.*, 2019, **480**, 979–989.
58 A. Olejnik, M. Ficek, K. Siuzdak and R. Bogdanowicz, *Electrochim. Acta*, 2022, **409**, 140000.
59 Z. S. Yan, Y. H. Zhang, H. Y. Yang, G. D. Fan, A. Ding, H. Liang, G. Li, N. Ren and B. Van der Bruggen, *Chem. Eng. Res. Des.*, 2020, **157**, 195–214.
60 L. C. Almeida, J. P. Correia and A. S. Viana, *Electrochim. Acta*, 2018, **263**, 480–489.
61 N. Li, Q. Y. Zhang, L. Han, J. T. Huang, X. D. Luo and X. B. Li, *Int. J. Hydrogen Energy*, 2023, **48**, 7004–7018.
62 J. Szewczyk, D. A. Ferrer and E. Coy, *Eur. Polym. J.*, 2022, **174**, 111346.
63 J. Kund, S. Daboss, T. M. D'alvise, S. Harvey, C. V. Synatschke, T. Weil and C. Kranz, *Nanomaterials*, 2021, **11**, 1964.